

Quantum tunneling of the Néel vector in antiferromagnetic $[3 \times 3]$ grid molecules

O. Waldmann*

Department of Chemistry and Biochemistry, University of Bern, CH-3012 Bern, Switzerland

(Dated: November 7, 2018)

Based on numerical calculations it is shown that the antiferromagnetic grid molecule Mn- $[3 \times 3]$ is a very promising candidate to experimentally detect the phenomenon of quantum tunneling of the Néel vector.

PACS numbers: 33.15.Kr, 71.70.-d, 75.10.Jm

Molecular nanomagnets such as Mn₁₂ and Fe₈ have attracted much interest as they show quantum tunneling of the magnetization at low temperatures.¹ For antiferromagnetic (AF) molecular wheels, a class of magnetic molecules in which an even number of ions is arranged in a ringlike fashion,² a different scenario associated with quantum tunneling of the Néel vector (QTNV) was predicted theoretically,³ but so far could not be observed experimentally. The identification of a magnetic molecule which enables the detection of QTNV would represent a major achievement, of interest also for applications in quantum technologies.

The experimental task to detect QTNV in molecular wheels is challenging: high sensitivity, low temperatures and strong magnetic fields are mandatory. A technique such as electron spin resonance (ESR) could meet these requirements, but does not couple to the Néel vector because of symmetry reasons.^{4,5} One way out would be to have a "sensor spin" which is coupled to only one of the AF sublattices.⁴ Its dynamics then will reflect the dynamics of the Néel vector. In principle, the nuclear spin of a metal center or a nearby proton might act as a sensor spin. Another solution would be to replace one of the magnetic ions on the ring by a dopant ion with different spin.⁶ The resulting excess spin also reflects the dynamics of the Néel vector - with the advantage of being detectable by ESR. Efforts in this direction are under way, but the synthesis of appropriate modified wheels is quite difficult.

Recently, a supramolecular Mn- $[3 \times 3]$ grid was investigated.^{7,8} Here, nine spin-5/2 Mn(II) ions occupy the positions of a regular 3×3 matrix, held in place by a lattice of organic ligands [see inset of Fig. 1(a)]. The unusual magnetic properties suggested that the $[3 \times 3]$ grid can be regarded as an AF "ring" doped with a central Mn ion.⁷ Indeed, the spin Hamiltonian of a $[3 \times 3]$ grid, which for an idealized structure reads⁹

$$H = -J_R \left(\sum_{i=1}^7 \mathbf{S}_i \cdot \mathbf{S}_{i+1} + \mathbf{S}_8 \cdot \mathbf{S}_1 \right) + D_R \sum_{i=1}^8 S_{i,z}^2 - J_C (\mathbf{S}_2 + \mathbf{S}_4 + \mathbf{S}_6 + \mathbf{S}_8) \cdot \mathbf{S}_9 + D_C S_{9,z}^2 + g\mu_B \mathbf{S} \cdot \mathbf{B}, \quad (1)$$

consists of a part involving only the ring of the eight peripheral metal ions, a part related to the central ion, and terms representing an interaction between these two sets of spin centers [\mathbf{S}_i is the spin operator of the i th ion with

spin $s = 5/2$, spins at "corners" are numbered 1, 3, 5, 7, those at "edges" 2, 4, 6, 8, and the central spin is numbered 9, see Fig. 1(a); z denotes the axis perpendicular to the grid plane]. For Mn- $[3 \times 3]$, an AF intraring coupling ($J_R < 0$) and uniaxial easy-axis anisotropy ($D_R < 0$) was found.^{7,8} Furthermore, the central spin is coupled to only one of the sublattices of the peripheral ring, namely to the edge spins. Thus, magnetically the Mn- $[3 \times 3]$ grid should correspond to an AF ring of eight spin-5/2 centers with a sensor spin naturally built in. This work demonstrates that Mn- $[3 \times 3]$ is indeed a promising molecule to detect QTNV experimentally.

The dimension of the Hilbert space is huge for Mn- $[3 \times 3]$. However, the low-energy sector of an AF ring (with a small, even number of sites N) is very well described by approximating the wave functions by $|\beta_A \beta_B S_A S_B S M\rangle$ with $S_A = S_B = Ns/2$.^{5,10,11} Here, S_A (S_B) denotes the total spin of sublattice A (B), and β_A , β_B abbreviate intermediate quantum numbers (omitted in the following). Physically, this approach works well because the internal spin structure due to the dominant Heisenberg interaction is essentially classical.¹² Applying this approximation to the ring terms in Eq. (1), an effective Hamiltonian for the Mn- $[3 \times 3]$ grid is obtained:

$$H_{eff}^{3 \times 3} = -\tilde{J}_R \mathbf{S}_A \cdot \mathbf{S}_B + \tilde{D}_R (S_{A,z}^2 + S_{B,z}^2) - J_C \mathbf{S}_A \cdot \mathbf{S}_9 + D_C S_{9,z}^2 + g\mu_B \mathbf{S} \cdot \mathbf{B}. \quad (2)$$

Here, $\tilde{J}_R = 0.526J$ and $\tilde{D}_R = 0.197D_R$. A (B) denotes the sublattice of corner (edge) spins. Figure 1 compares results calculated for $H_{eff}^{3 \times 3}$ and H . The agreement is quite good. $H_{eff}^{3 \times 3}$ is designed to reproduce the lowest-lying states optimally, higher-lying states are thus increasingly less well described.

Remarkably, $H_{eff}^{3 \times 3}$ works well in a wide range of $J_C/|J_R|$ values. In the strong coupling limit, $|J_C| \gg |J_R|$, the wave functions should be approximated by $|S_B S_9 S_{B9} S_A S M\rangle$, i.e., by coupling first the spins S_B and S_9 , and then the resulting spin S_{B9} with S_A . In the weak coupling limit, however, the appropriate wave functions would be $|S_A S_B S_{AB} S_9 S M\rangle$, where first S_A and S_B are coupled together. As both wave functions lead to the same effective Hamiltonian, Eq. (2), a broad range of $J_C/|J_R|$ is covered. This suggests a general strategy to construct an effective Hamiltonian: Sublattices as expected from the classical spin configuration are introduced, and then spins of each sublattice are replaced

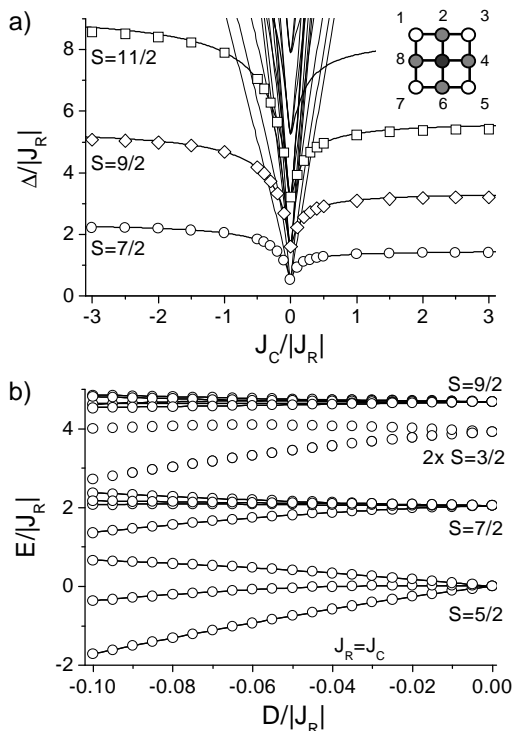


FIG. 1: (a) Energies of the low-lying states with respect to the $S = 5/2$ ground state as function of J_C for $H_{eff}^{3 \times 3}$ (lines) and H (symbols) with $D_R = D_C = 0$ in zero field. For H , only the energy gaps for the lowest states with $S = 7/2, 9/2, 11/2$ are displayed. The inset shows the structure of the Mn-[3 × 3] grid schematically. (b) Energy spectrum for $H_{eff}^{3 \times 3}$ (lines) and H (circles) as function of $D \equiv D_R = D_C$ for $J_C = J_R$ at zero field. The spin multiplets get split by the anisotropy. The $S = 5/2$ level for instance split in the sequence $|M| = 1/2, 3/2, 5/2$. Twofold degenerate spin levels such as the $S = 3/2$ levels at about $3.5|J_R|$ are not reproduced by $H_{eff}^{3 \times 3}$. They belong to an E band similar as in wheels,^{10,12} but are not relevant here as explained in the text.

by the mean-field spin $\mathbf{S}_{SL} = 1/N_{SL} \sum_{i \in SL} \mathbf{S}_i$ (N_{SL} denotes the number of spins of sublattice SL). The effect of weak quantum fluctuations may be accounted for by renormalizing the parameters of the effective Hamiltonian, hence J_R and \tilde{D}_R in Eq. (2).⁵

Interestingly, a similarity of the single-molecule magnet Mn_{12} ^{1,13} and a [3 × 3] grid turns up: Mn_{12} may be regarded as an octanuclear ring of Mn(III) ions doped by a central Mn(IV) tetramer. The above considerations then lead directly to an effective Hamiltonian, which, in view of the success of this approach for the molecular wheels and the [3 × 3] grid, is expected to describe also the relevant states of Mn_{12} well.

With $H_{eff}^{3 \times 3}$, QTNV in Mn-[3 × 3] can now be readily analyzed numerically. The energy spectrum as function of magnetic field is shown in Fig. 2 for several field orientations and $J_R = J_C = -5$ K, $D_R = D_C = -0.14$ K (θ denotes the angle between magnetic field and z axis; the azimuthal angle φ has no effect, as is evident from H ,

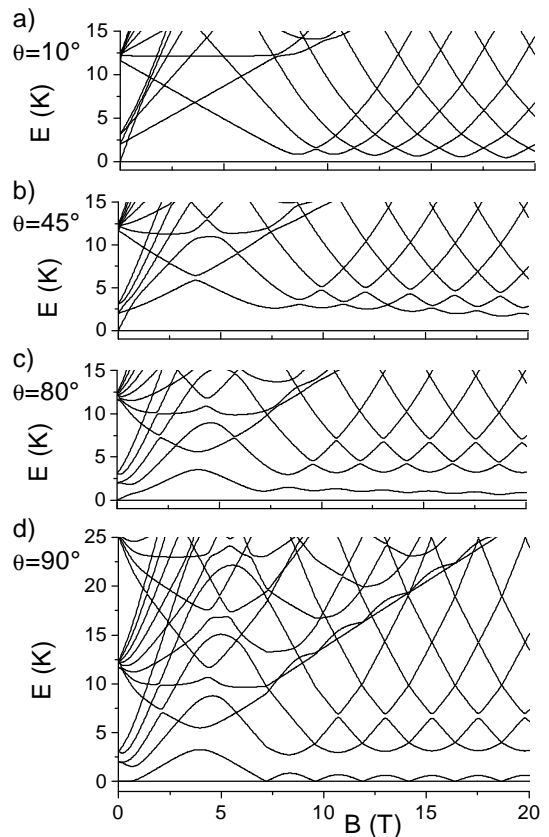


FIG. 2: Energy spectrum vs magnetic field for different orientations θ of the magnetic field (the energy of the lowest state was set to zero at each field). For zero field, the states with energy below 3 K belong to the $S = 5/2$ ground state multiplet (which exhibits a hard-axis zero-field splitting), those at ≈ 12.5 K to the next higher $S = 7/2$ multiplet, and those at ≈ 25 K to the $S = 9/2$ multiplet.

$H_{eff}^{3 \times 3}$). These parameters are supported by recent inelastic neutron scattering experiments,¹⁴ and torque measurements at very low temperatures.⁸ The semiclassical tunneling action $S_0/\hbar = NS_i \sqrt{2D_R/J}$ (QTNV sets in for $S_0/\hbar \gg 1$, see Ref. 3) is then estimated to $S_0/\hbar = 4.7$, which is even larger than for Fe_{10} ($S_0/\hbar = 3.3$) and CsFe_8 ($S_0/\hbar = 3.9$).^{5,6} This demonstrates that Mn-[3 × 3] is indeed a favorable candidate with respect to QTNV. Some following points should be noted:

1) Concerning the dependence on $J_C/|J_R|$, the states should be divided into the energetically lowest states for $S = 5/2, 7/2, 9/2, \dots$, and the remainder of the states (in the terminology of Refs. 10 and 12, these states form the L band, while the remaining states belong to either the E band or the quasicontinuum). Obviously, only the first set of states (the L band) is relevant for the low-lying part of the energy spectrum in magnetic fields. As soon as J_C assumes significant values, the relative energy spacings of these states, and therewith the relative field positions of the ground-state level crossings, are close to those found in the strong-coupling limit $|J_C| \gg |J_R|$, even if $|J_C|$ is

much smaller than $|J_R|$. The weak-coupling limit is realized only for $|J_C/J_R| \lesssim 0.002$. Thus, the results shown in this work for $J_C = J_R$ are actually characteristic for the strong coupling limit.

2) The energy gap between ground and first excited state, $\Delta(B)$, shows a $|\sin(\pi g \mu_B B/J_R + \alpha)|$ -like oscillatory field dependence for high fields in the grid plane [Fig. 2(d)]. Such a behavior was identified as a characteristic of QTNV in the (modified) molecular wheels.^{3,6} α accounts for a shift in field.

3) Finally, $\Delta(B)$ periodically drops to zero indicating level crossings (LCs) at fields B_m ($m \in \mathbb{N}$).^{5,11} Such LCs trivially exist for $\theta = 0^\circ$. However, for canted magnetic fields gaps appear at each LC field, i.e., the ground state LCs become anticrossings signaling level mixing (Fig. 2). Starting with $\theta = 0^\circ$, the gaps at the LC fields first increase, reach maximal values at around $\theta = 45^\circ$, and then shrink to disappear again at $\theta = 90^\circ$. In the (unmodified) wheels, $\Delta(B_m) = 0$ is enforced by symmetry for all field directions.^{5,11} This symmetry is absent in $[3 \times 3]$ grids, and for fields with $\theta \neq 0^\circ$ gaps open at the LCs due to the action of the uniaxial magnetic anisotropy: In a coordinate frame with z' parallel to the field, one obtains $DS_z^2 = D'S_z'^2 + E'(S_x'^2 - S_y'^2) - G'(S_x'S_z' + S_z'S_x')$. The G' term mixes the two levels involved in a LC (for which $|\Delta M'| = 1$), leading to the above behavior as $G' = \sin(\theta) \cos(\theta) D/3$. This angular behavior of $\Delta(B)$ has important implications for the QTNV scenario (*vide infra*).

In order to analyze QTNV, the matrix elements between the ground state $|0\rangle$ and the 20 next higher lying states $|n\rangle$ were calculated for the z component of the Néel vector $|\langle 0|N_z|n\rangle|$, the total spin $|\langle 0|S_z|n\rangle|$, and the central spin $|\langle 0|S_{9,z}|n\rangle|$ ($n = 1, \dots, 20$ numbers the states by their energy at each field). The Néel vector was defined as $\mathbf{N} = \mathbf{S}_A - \mathbf{S}_B + \mathbf{S}_9$. The results as function of magnetic field are shown in Figs. 3(a)-(c) for $\theta = 90^\circ$.

For the Néel vector, the excitation between ground and first excited state, $|\langle 0|N_z|1\rangle|$, which corresponds to QTNV, is dominant [Fig. 3(a)]. The energy gap $\Delta(B)$ is thus identified as the tunneling gap due to QTNV (for fields beyond the first LC). Higher-lying excitations, in particular, to the second excited state, are also present. Accordingly, the correlation function vs time, $\langle 0|N_z(t)N_z(0)|0\rangle \propto \sum_n |\langle 0|N_z|n\rangle|^2 \exp(-\frac{i}{\hbar}E_n t)$, shows a dominant oscillation at the tunneling frequency Δ/\hbar disturbed by higher frequent oscillations. As the contribution of higher-lying excitations is minimal for magnetic fields inbetween LCs [where the tunneling gap $\Delta(B)$ assumes maxima, see Fig. 2(d)], the dynamics of the Néel vector is best described by QTNV at these fields.

In S_z , three excitations have significant intensities [Fig. 3(b)]. The excitation with maximum at ≈ 1 T corresponds to a transition within the $S = 5/2$ ground-state multiplet. The excitation gaining increasing intensity from ≈ 5 T onwards corresponds to a transition to the Zeeman-split level, which is visible in the energy spectrum at energies $\approx g\mu_B B$ [Fig. 2(d)]. And finally, the

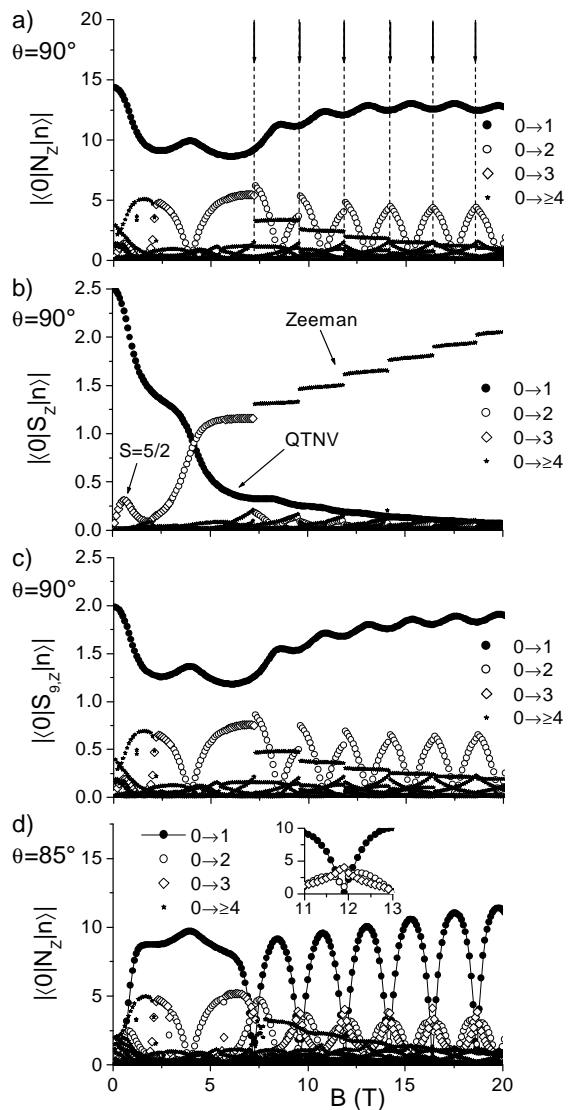


FIG. 3: Absolute matrix elements between the ground and the 20 next higher-lying states for the z component of (a) the Néel vector, (b) the total spin, and (c) the central spin for fields in the plane of the grid. Arrows and dashed lines in panel (a) indicate the positions of LCs. (d) Matrix elements for the Néel vector for slightly canted field. The inset magnifies the field range 11 - 13 T for the first three matrix elements.

excitation with an approximate B^{-2} field dependence corresponds to the transition between the ground and first excited state reflecting exactly QTNV.⁶

The matrix elements for the central spin basically just behave as those of the Néel vector [Fig. 3(c)]. This is of course expected, but demonstrates unambiguously that the central spin of a $[3 \times 3]$ grid indeed acts as a sensor spin for the dynamics of the spins on the peripheral ring.

The results resemble those for molecular wheels: The field dependencies of $\Delta(B)$, $|\langle 0|S_z|1\rangle|$, $|\langle 0|N_z|1\rangle|$ (and $|\langle 0|N_z|2\rangle|$) show similar behavior as for the modified and unmodified wheels.^{6,11} As shown above, the strong cou-

pling limit is effectively realized in Mn-[3 × 3]. Then the sublattice spin S_B and the central spin S_9 act as a combined larger spin S_{B9} , and $H_{eff}^{3 \times 3}$ simplifies to $H' = -J' \mathbf{S}_A \cdot \mathbf{S}_{B9} + D'_A S_{A,z}^2 + D'_B S_{B9,z}^2 + g\mu_B \mathbf{S} \cdot \mathbf{B}$, which is exactly the effective Hamiltonian of a modified wheel.⁶ Thus, magnetically Mn-[3 × 3] behaves like a modified AF wheel.

The new feature observed here is that, along with the opening of gaps at the LCs, the behavior of the matrix elements changes drastically for $\theta \neq 0, 90^\circ$, Fig. 3(d) (preliminary calculations confirmed similar behavior for the modified wheels). At the LC fields, $|\langle 0|N_z|1\rangle|$ (and $|\langle 0|N_z|2\rangle|$) vanishes and $|\langle 0|N_z|3\rangle|$ becomes the dominant matrix element. Apparently, the opening of gaps at the LCs and the rise of $|\langle 0|N_z|3\rangle|$ results in a breakdown of the QTNV scenario at these fields. Thus, the picture of QTNV needs an extension near LCs in the case of Mn-[3 × 3] or modified wheels. However, importantly, in those regions of the magnetic field where the tunneling gap $\Delta(B)$ is large, QTNV persists even for sizeable canting angles.

Finally, the prospects of an experimental observation of QTNV in Mn-[3 × 3] is discussed. Having shown that the central spin acts as sensor spin and the analogy with a modified wheel, the considerations of Refs. 4,6 are applicable to Mn-[3 × 3]. Only main points will be addressed here, further details may be found in these works.

QTNV can be detected by the highly sensitive ESR technique, as is evident from Fig. 3(b) noting that the ESR intensity is proportional to $|\langle 0|S_z|1\rangle|^2$ for $\theta = 90^\circ$. For Mn-[3 × 3], the most favorable field regime would be 10-20 T, see Fig. 3(a). In this regime, the ESR intensity is smaller by two orders of magnitude compared to the maximal intensity at $B = 0$, but is still large enough to be detectable with today's ESR spectrometers, especially as rather large high-quality single crystals are available.¹⁵ The magnetic field should be oriented close to the plane of the grid, but a canting of about 5° is well tolerable

if QTNV is measured near the tops of the tunneling gap $\Delta(B)$, i.e., at fields inbetween LCs. In a continuous-wave ESR experiment, the linewidth of the signal provides an upper limit for the decoherence rate Γ_S , which allows one to test the coherence condition $\Gamma_S < \Delta/\hbar$, or if QTNV in Mn-[3 × 3] is coherent, respectively.⁴

Nuclear magnetic resonance (NMR) experiments are an alternative. As shown in Ref. 4, QTNV leads to an absorption peak in the NMR signal at $\omega = \Delta/\hbar$, but with an intensity significantly reduced as $(A/\Delta)^2$ (A is the hyperfine coupling constant). For molecular wheels it was suggested to measure near LCs, where Δ is small, in order to gain intensity. But for Mn-[3 × 3], this would require an unrealistically accurate orientation of the magnetic field perpendicular to the grid plane. Fortunately, the sensitivity of Mn⁵⁵-NMR is 3×10^5 times larger than of Fe⁵⁷-NMR,¹⁶ resulting in detectable signals also near the maxima of $\Delta(B)$ in Mn-[3 × 3]. And, as mentioned already, relatively large single crystals are available.¹⁵ It is added that the NMR signal due to QTNV can be easily identified by its field dependence which differs markedly from that of the Lamor frequency.

In conclusion, the molecular grid Mn-[3 × 3] is an exciting prospect for observing quantum tunneling of the Néel vector experimentally: It has a sensor spin naturally built in which enables a detection of tunneling by ESR, and it features the highest value of the tunneling action S_0/\hbar known to date. The issue of coherence is of great importance for any potential applications. In view of tunneling gaps of 1 K, coherent QTNV might be realized in Mn-[3 × 3].

Acknowledgments

I thank F. Meier for many enlightening discussions on the subject.

* Electronic address: waldmann@iac.unibe.ch

¹ D. Gatteschi and R. Sessoli, *Angew. Chem. Int. Ed.* **42**, 268 (2003).

² K. L. Taft, C. D. Delfs, G. C. Papaefthymiou, S. Foner, D. Gatteschi, and S. J. Lippard, *J. Am. Chem. Soc.* **116**, 823 (1994); D. Gatteschi, A. Caneschi, L. Pardi, and R. Sessoli, *Science* **265**, 1054 (1994).

³ A. Chiolero and D. Loss, *Phys. Rev. Lett.* **80**, 169 (1998).

⁴ F. Meier and D. Loss, *Phys. Rev. Lett.* **86**, 5373 (2001).

⁵ O. Waldmann, *Europhys. Lett.* **60**, 302 (2002).

⁶ F. Meier and D. Loss, *Phys. Rev. B* **64**, 224411 (2001).

⁷ O. Waldmann, L. Zhao, and L. K. Thompson, *Phys. Rev. Lett.* **88**, 066401 (2002).

⁸ O. Waldmann, S. Carretta, P. Santini, R. Koch, A. G. M. Jansen, G. Amoretti, R. Caciuffo, L. Zhao, and L. K. Thompson, *Phys. Rev. Lett.* **92**, 096403 (2004).

⁹ Intramolecular dipole-dipole interactions are not negligible, but have similar effects as the single-ion anisotropy

and are well grasped by $S_{i,z}^2$ terms. The D values should be understood as to include both anisotropy contributions.

¹⁰ O. Waldmann, *Phys. Rev. B* **65**, 024424 (2002).

¹¹ A. Honecker, F. Meier, D. Loss, and B. Normand, *Eur. Phys. J. B* **27**, 487 (2002).

¹² O. Waldmann, T. Guidi, S. Carretta, C. Mondelli, and A. L. Dearden, *Phys. Rev. Lett.* **91**, 237202(2003).

¹³ N. Regnault, Th. Jolicoeur, R. Sessoli, D. Gatteschi, and M. Verdager, *Phys. Rev. B* **66**, 054409 (2002).

¹⁴ T. Guidi, S. Carretta, P. Santini, E. Livioti, N. Magnani, C. Mondelli, O. Waldmann, L. K. Thompson, L. Zhao, C. D. Frost, G. Amoretti, and R. Caciuffo, *Phys. Rev. B* **69**, 104432(2004).

¹⁵ L. K. Thompson, private communication.

¹⁶ J. N. S. Evans, *Biomolecular NMR Spectroscopy* (Oxford University Press, Oxford, 1995).